

Thermoelectric properties of Topological Weyl Semimetal $\text{Cu}_2\text{ZnGeTe}_4$

Bhawna Sahni,¹ Riddhimoy Pathak,² P C Sreeparvathy,¹
Tanusri Saha-Dasgupta,³ Kanishka Biswas,² and Aftab Alam^{1*}

¹*Materials Modelling Group, Department of Physics,*

Indian Institute of Technology, Bombay, Powai, Mumbai 400 076, India

²*New Chemistry Unit, International Centre for Materials Science and School of Advanced Materials,
Jawaharlal Nehru Centre for Advanced Scientific Research (JNCASR), Jakkur P.O., Bangalore, 560064, India and*

³*Department of Condensed Matter and Materials Physics,
S. N. Bose National Centre for Basic Sciences, JD Block,
Sector III, Salt Lake, Kolkata, West Bengal 700106, India*

(Dated: June 21, 2023)

The study of topological quantum materials for enhanced thermoelectric energy conversion has received significant attention recently. Topological materials (including topological insulators and Dirac/Weyl/nodal-line semi-metals) with unique nature of band structure involving linear and regular parabolic bands near Fermi level (E_F) have the potential to show promising TE properties. In this article, we report the promising TE performance of a quaternary chalcogenide ($\text{Cu}_2\text{ZnGeTe}_4$) having non-trivial topological phase. At ambient condition, the compound is a narrow band gap (0.067 eV) semiconductor, with a TE figure of merit (ZT) 1.2. Application of 5% strain drives the system to a topologically non-trivial Weyl semi-metal with the right combination of linear and parabolic bands near E_F , giving rise to a reasonable ZT of 0.36. Apart from strain, alloy engineering (Sn substituted at Ge) is also shown to induce topological non-triviality. The present work demonstrates the potential of such unique semimetals for exceptional electronic transport properties and hence excellent thermoelectric performance.

I. INTRODUCTION

Thermoelectric (TE) materials are energy-harvesting materials that have been at the forefront of condensed matter research for decades.^{1–9} The TE energy conversion efficiency is governed by a dimensionless figure of merit (ZT) which depends on different transport coefficients as $ZT = S^2\sigma/(\kappa_e + \kappa_L + \kappa_b)$ where S is the Seebeck coefficient, σ is electrical conductivity, κ_e and κ_L are electronic and phononic components of thermal conductivity while κ_b is its bipolar component whose contribution becomes appreciable when minority charge carriers also start contributing to the transport. By using either hierarchical phonon scattering^{10,11} or phonon engineering¹², it is possible to efficiently obstruct the propagation of heat-carrying phonons to suppress the κ_L values of most of the TE materials. However, enhancing the power-factor ($S^2\sigma$) is necessary for further improvement of ZT. The challenge in achieving that is mainly associated with strong coupling between the electronic transport coefficients.¹³ Careful band engineering has been proven to be successful to enhance the electronic transport of TE materials by decoupling these coefficients.^{14,15}

In recent years, the coexistence of thermoelectric properties with topological non-trivial features gathered enormous attention. In fact, a large number of TEs have been reported to be excellent TI materials, for e.g., bismuth telluride (Bi_2Te_3), antimony telluride (Sb_2Te_3), bismuth selenide (Bi_2Se_3), tin telluride (SnTe), etc.^{16–20} They are found to have similarities, such as presence of a heavy element and a narrow band gap. The strong spin-orbit coupling (due to heavy elements) opens up the band gap

between the inverted bands, thus forming the topological states, leading to complex bulk bands which are beneficial for TE performance.²¹ The presence of heavy element helps in the reduction of lattice thermal conductivity. However, in TIs, it is crucial to tune the E_F to bring it into the forbidden gap so that topological surface states can dominate the transport properties, keeping the bulk bands insulating. On the other hand, high TE performance is achieved when bulk bands contribute dominantly to the electronic transport properties. It is quite challenging experimentally to have a system with well-modulated E_F so as to observe topological surface-state dominated transport properties. Thus, robust topological states in bulk are new prospects in thermoelectrics.

Topological semi-metals (TSM) (e.g. Dirac and Weyl semi-metals)²² are 3D analogs of graphene, having gapless electronic excitations which are protected by topology as well as symmetry. These semi-metals also show topological surface states similar to topological insulators along with peculiar bulk bands. This provides a new platform for the realization of exotic transport properties. However, semi-metals in general show small thermopower due to bipolar conduction which makes these materials less useful for TE applications. Recently, there are a few studies where semi-metals have been explored to achieve promising thermoelectric properties.^{23,24} A semi-metal is expected to facilitate good TE properties if it hosts both parabolic and linearly dispersed bands near the Fermi level enabling an appreciable difference in the number of majority and minority carriers to reduce the bipolar effects. Fig 1 illustrates such band convergence criteria which acquire both heavy band and a featured band or regular band and featured band near the Fermi-level

(E_F). At a fixed carrier concentration, the dispersive bands will give a small effective band mass giving rise to high carrier mobility while the flat bands have large density of states which will give large Seebeck coefficient. Thus, semi-metals which contains a combination of both regular parabolic and featured bands near E_F can be quite beneficial for promising TE properties. This has the potential to make some of the Dirac/Weyl semi-metals promising candidates for TE applications. The family of chalcogenides are the appropriate choice to realize such combination of bands.

Chalcogenides, in general, have gathered enormous attention due to their wide applications, such as those in solar energy²⁵, batteries²⁶, thermoelectric devices²⁷ as well as topological insulators¹⁶. Among these, quaternary chalcogenides in particular, have emerged as promising candidates for photovoltaics²⁸, electrocatalysis²⁸ and topological insulators²⁹. Though a large number of studies on various individual properties are reported in the literature, a detailed study, involving the presence of non-trivial topological phase and thermoelectric properties is lacking. The copper based quaternary chalcogenides consist of two structural units, out of which one is electrically insulating [Cu_2X_4] while the other is conducting [ABX_4]³⁰ where X= S, Se, Te and A is transition metal element while B is a group IV element. These structures are naturally distorted which results in lower values of lattice thermal conductivity.³¹ However, since quaternary alloys exhibit substantially wider band gaps (for instance, $\text{Cu}_2\text{ZnSnSe}_4$ has 1.41 eV band gap and $\text{Cu}_2\text{CdSnSe}_4$ has 0.98 eV),³² these alloys show inferior electronic transport properties in comparison to conventional alloy materials. Further due to the presence of heavy bands, the carriers have low mobility. Thus, these compounds have lower electrical conductivity due to wide band gap and low carrier mobility.

In this letter, we report a combined theoretical and experimental study of a new quaternary chalcogenide $\text{Cu}_2\text{ZnGeTe}_4$. At ambient condition (experimental structure), it shows a narrow band gap semiconducting phase ($E_g = 0.067$ eV) with reasonably appreciable $ZT = 1.2$. The spin-orbit coupling (SOC) plays a vital role in reducing the band gap and hence increasing the electrical conductivity. Thus, promising electronic transport properties are achieved as compared to previously reported quaternary alloys. Expanding the lattice by a small amount (or theoretically optimized structure) transform the compound to a topological Weyl semi-metal, still with reasonably acceptable TE properties ($ZT \sim 0.36$). Topological non-trivial property of this phase is confirmed by band inversion, opposite chirality and robust surface states. The coexistence of TE and topological properties are mainly governed by the simultaneous occurrence of regular parabolic and featured bands, as confirmed from the topology of our calculated band structures. We have also demonstrated the coexistence of TE and TI properties in Sn-substituted $\text{Cu}_2\text{ZnGeTe}_4$, which effectively expand the unit cell volume and hence induce

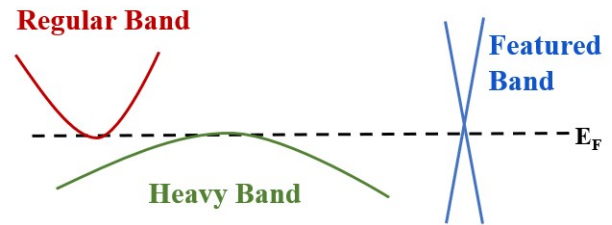


FIG. 1. Schematics of different band features whose coexistence are useful for promising thermoelectric performance.

Lattice parameter	Theoretical	Experimental ⁴⁵
a = b (Å)	6.105	5.999
c (Å)	12.09	11.918
Volume (Å ³)	450.55	428.91

TABLE I. Theoretically optimized and experimental lattice parameters for $\text{Cu}_2\text{ZnGeTe}_4$

the TE properties.

II. METHODS

First-principles calculations were performed using Vienna *Ab-initio* simulation package (VASP)^{34–36} package with a projector augmented wave⁴² basis and the generalized gradient approximation (GGA)³⁷ exchange-correlation functional of Perdew–Burke–Ernzerhof (PBE).^{39,40} Further computational details are provided in the Supplementary Material (SM).⁴⁸

III. RESULTS AND DISCUSSIONS

A. Crystal structure

$\text{Cu}_2\text{ZnGeTe}_4$ crystallizes in tetragonal symmetry with space group $I\bar{4}2m$ (#121) (D_{2d} point group)(See Fig. 2(a)). It preserves the time-reversal symmetry but breaks the inversion symmetry. It has two formula units leading to 16 atoms in the unit cell. All quaternary compounds have the tetragonal lattice structure, often known as the low-symmetry non-cubic structure. The structure can also be visualized as the supercell of the zinc-blende structure along the z-direction where three different type of cations (Cu, Zn, Ge) are substituted at the zinc site and sulphur is replaced by tellurium. Every atom has a tetrahedral surrounding and the tetrahedron is made of tellerium and metal cations. Four metal atoms surround each tellurium atom. Anionic Te atoms are found inside the tetrahedral void formed by cationic elements. The difference in electronegativity between the cations and the different interatomic distances lead to a naturally occurring superlattice structure with localised lattice distortions. Between the cations and Te anions, the

complex structure exhibits various bonding lengths and bonding angles. The bonding lengths between these three different cations and the Te anions are Zn-Te = 2.695 Å, Ge-Te = 2.691 Å, Cu-Te = 2.576 Å in a tetrahedron. Thus, it forms a locally distorted kind of anionic framework. Table I shows the experimental and theoretically optimized lattice parameters for this compound. The theoretically optimized structure can also be seen as $\sim 5\%$ hydrostatically expanded structure with respect to the experimental unit cell volume. Interestingly, such a small hydrostatic expansion shows a profound effect on the structure with drastic changes in the electronic structure. We shall report a detailed study of $\text{Cu}_2\text{ZnGeTe}_4$ at both these volumes and discuss the contrasting features.

B. Electronic structure

Figure 3(a,b) shows the band structure and density of states of $\text{Cu}_2\text{ZnGeTe}_4$ at experimental lattice parameters. It shows an indirect band gap of 0.067 eV. The most dominant contribution to the conduction bands arises from Te p-orbitals while that to valence bands arise from Cu d-orbitals and Te p-orbitals. Conduction band minima (CBM) occur at X point, while valence band maxima (VBM) occur at Γ point making it an indirect band gap semiconductor. There is yet another minima in the conduction band at Γ point slightly above the one at X-point. The low band gap and the presence of multiple bands near the Fermi level are the preliminary signatures of promising transport properties.

In contrast, $\text{Cu}_2\text{ZnGeTe}_4$ shows semi-metallic feature at the theoretically optimized volume (See Fig. 3(c)). Interestingly, it also exhibits a band inversion around Γ point originating from the flipping of 's' character, representing the topological non-trivial nature. The system transforms from a topologically trivial to a non-trivial phase along with the semiconductor to a semi-metallic phase due to hydrostatic volume expansion. Broken inversion symmetry gives rise to the possibility of Weyl nodes. A search in the entire Brillouin zone (BZ) revealed

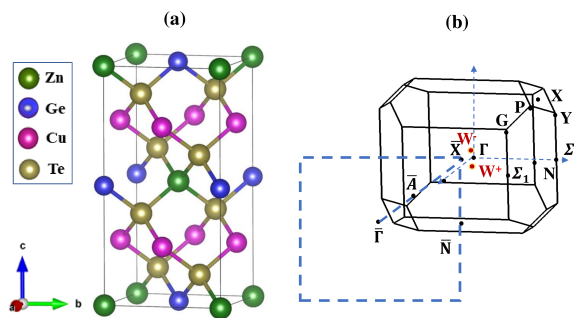


FIG. 2. For $\text{Cu}_2\text{ZnGeTe}_4$, (a) crystal structure with space group $I\bar{4}2m$ (#121) (b) Bulk and (001) surface Brillouin zones. Weyl points are labelled as W^+ and W^-

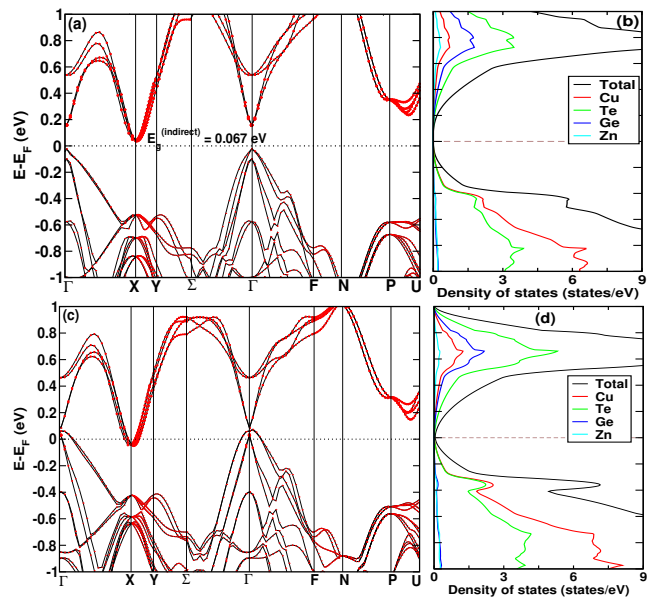


FIG. 3. For $\text{Cu}_2\text{ZnGeTe}_4$, electronic band structure and atom-projected density of states at (a,b) experimental volume (c,d) theoretically optimized volume. The former is a narrow band gap semiconductor while the latter is a Weyl semi-metal. Red circles indicate s-states. Fermi level (E_F) is set at 0 eV.

the presence of two Weyl points near the Γ point labeled as W^+ , W^- whose coordinates are shown in Table II. The bulk band dispersion around these two Weyl points are shown in Fig. 4(a,b). These Weyl points have opposite chirality and obey the Nielsen-Ninomiya theorem.⁴⁶ The location of these Weyl points is slightly above the Fermi level as shown in Figure 4(a,b). The corresponding Berry curvature around these points showing the source and sink nature are presented in Fig. 4(c,d). Surface states are very important feature for a topological material. Since, this compound shows Weyl nodes in the bulk band structure, it is expected to host a robust surface state originating from this bulk Weyl point. The surface

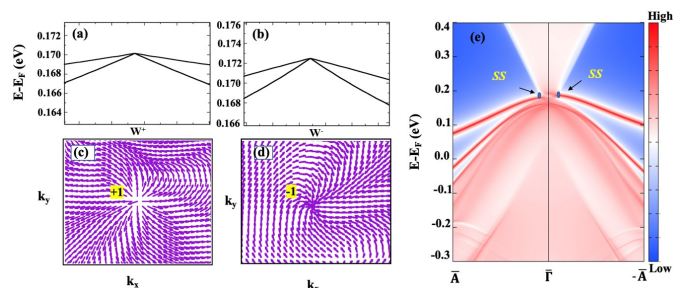


FIG. 4. For $\text{Cu}_2\text{ZnGeTe}_4$ (in semi-metallic state), (a,b) zoomed-in view of bulk band structure around Weyl points W^+ and W^- (c,d) Berry curvature around W^+ and W^- with chirality +1 and -1 respectively, (e) surface band structure projected along (001) direction.

Points	k_x	k_y	k_z	Chirality
W^+	0.00155	0.00693	0.02230	+1
W^-	0.00794	-0.00320	-0.02663	-1

TABLE II. For $\text{Cu}_2\text{ZnGeTe}_4$ (in semi-metallic state), coordinates of Weyl points in the reciprocal space with opposite chirality.

band structure projected on the (001) surface is shown in Figure 4(e) which clearly shows two Weyl points at around Γ point.

C. Phonon properties

Phonons play a crucial role in dictating various novel properties of a material. $\text{Cu}_2\text{ZnGeTe}_4$ contains 2 formula units including 16 atoms leading to a total of 48 phonon bands in the phonon spectrum, as shown in Figure 5(a) for the semiconducting phase. Among them, three bands originate from acoustic phonon branches while the rest 45 bands represent the optical phonon modes. Interestingly this compound facilitates various phonon band crossings in both acoustic and optical phonon frequencies. A close observation of the acoustic region reveals highly entangled acoustic and low-frequency optical modes, which eventually helps to reduce lattice thermal conductivity and are hence beneficial for thermoelectric applications. Atom projected phonon density of states shown in Figure 5(b), helps to identify the contribution of different atoms in different frequency ranges of the phonon spectra. The heavy element ‘Te’ contributes in the low frequency acoustic region while the other three elements shows up at a relatively high frequency.

Figure SI (in SM⁴⁸) shows the phonon dispersion nd atom-projected phonon density of states for the semi-conducting state at low frequencies. The eigenmode displacements of few of the low-frequency modes is shown in the bottom panel of Fig. 5. The predominant vibrations arises from Te-atoms, followed by Cu. The mixing of the acoustic and optical phonon modes can be seen in 3rd, 4th, 5th and 6th bands at X, N and P high symmetry points. The change in phonon mode frequencies with slight changes in volume is explained by the frequency dependence of mode gruneisen parameter (γ), which is shown in Fig. 5(c). In other words, γ is a measure of the anharmonicity of the lattice; the higher the γ -value, the more anharmonic the lattice is; which causes more scattering and hence lowers the κ_L values. At low frequencies, phonons, particularly the acoustic modes, show negative values of mode gruneisen parameter which could be due to the special structure framework where the anions are at the middle of the tetrahedral void and the corners are shared by cations. At low frequencies, transverse displacement of the anion (Te) atom causes other cationic atoms in the void to shrink towards each other.⁴⁷

The semi-metallic phase of $\text{Cu}_2\text{ZnGeTe}_4$ acquires simi-

lar phonon spectra and Gruneisen parameter values. Figure 5(d) shows the lattice thermal conductivity (κ_L) for semiconducting and semi-metallic state of $\text{Cu}_2\text{ZnGeTe}_4$. Semiconducting phase shows lower values of κ_L because of a more entangled acoustic and optical phonon branches in the low frequency range, as well as a more compact locally distorted anionic framework.

D. Thermoelectric properties

Band topology plays a crucial role in governing the transport properties, and in turn, the TE performance of a material. Band convergence¹⁴ is a clever strategy to improve TE performance which is quite evident in $\text{Cu}_2\text{ZnGeTe}_4$. There are regular parabolic bands in both the conduction and valence side of the band structure along with the light bands (see Figure 3). This maximizes both Seebeck coefficient and electrical conductivity in this material. Along with that, low values of thermal conductivity further helps to enhance the TE figure of merit. In the following subsections, we will describe the thermoelectric properties of $\text{Cu}_2\text{ZnGeTe}_4$ in both semi-conducting (experimental volume) and semi-metallic (theoretical volume) states.

1. Semi-conducting state:

The transport properties are calculated by taking into account different scattering effects namely, acoustic deformation potential (ADP), ionized impurity (IMP), polar optical phonon (POP) and piezoelectric (PIE) scattering within the ab-initio framework.⁴⁴ The total relaxation time (τ) values for semiconducting $\text{Cu}_2\text{ZnGeTe}_4$ at different values of carrier concentrations and temperatures for p-type and n-type conduction are shown in SM.⁴⁸ The value of τ at room temperature is around ~ 80 fs for holes and around ~ 60 fs for electrons. Figure 6 shows the variation of electrical conductivity (σ), power factor ($S^2\sigma$), electronic thermal conductivity (κ_e) and thermoelectric figure of merit (ZT) with respect to carrier concentration at different temperatures for p-type (left) and n-type (right) conduction for $\text{Cu}_2\text{ZnGeTe}_4$. The compound shows higher σ values for n-type conduction due to linearly dispersive nature of conduction bands. These values are quite high as compared to other copper-based quaternary chalcogenides ($\text{Cu}_2\text{B}^{\text{II}}\text{C}^{\text{IV}}\text{X}_4$) which show conductivity in the range $10^3 - 10^4$ (S/m). The higher values of κ_e at lower concentrations and high temperatures are due to bipolar conduction.⁴⁹

The maximum value of ZT in the semiconducting phase is 0.87 and 1.2 for p-type and n-type conduction respectively at 500 K. At a fixed value of carrier concentration of $1 \times 10^{20} \text{ cm}^{-3}$ at which ZT is maximum, the value of S, σ and $S^2\sigma$ is $158.25 \mu\text{V/K}$, $2.69 \times 10^5 \Omega^{-1}\text{m}^{-1}$ and $6.74 \text{ mWm}^{-1}\text{K}^{-2}$ respectively for p-type conduction. The same for n-type conduction are 178.62

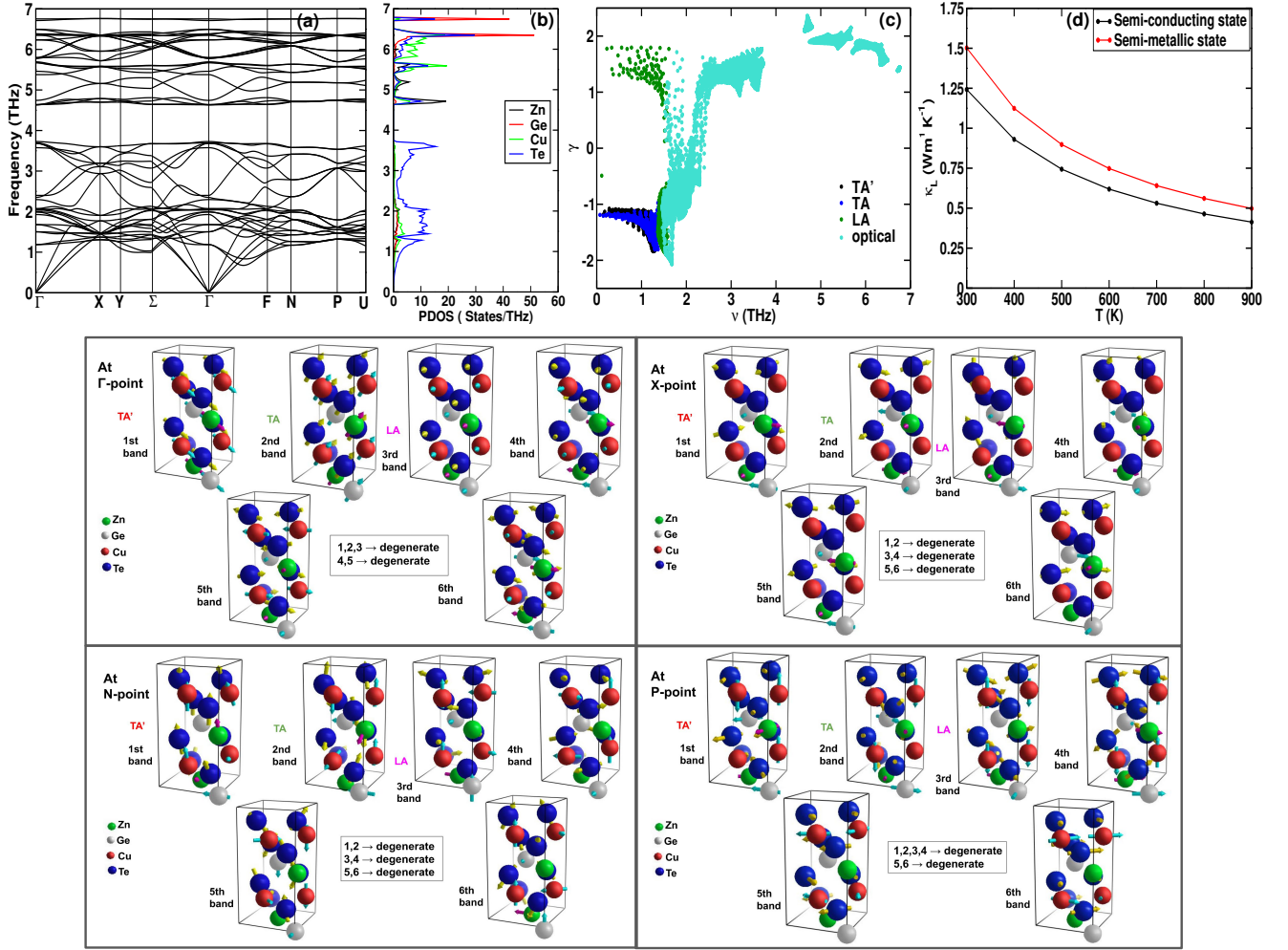


FIG. 5. For $\text{Cu}_2\text{ZnGeTe}_4$, (Top)(a,b) phonon dispersion, atom-projected phonon density of states and (c) the mode Gruneisen parameter (γ) for semiconducting phase. (d) lattice thermal conductivity (κ_L) for semi-conducting and semi-metallic state. (Bottom) Visualization of acoustic and soft phonon modes at Γ , X, N and P high symmetry points

$\mu\text{V/K}$, $3.21 \times 10^5 \Omega^{-1}\text{m}^{-1}$ and $10.4 \text{ mWm}^{-1}\text{K}^{-2}$ at a carrier concentration of $4 \times 10^{19} \text{ cm}^{-3}$. It can be seen that the values of S and σ are higher in the case of n-type leading to a higher power factor as compared to p-type conduction. This is due to the presence of highly dispersive conduction bands at Γ point and four-fold degenerate regular bands at X point. Thus, σ as well as S values are high for n-type conduction.

2. Semi-metallic state

Topological semi-metals such as Weyl/Dirac materials can offer a perfect combination of light and heavy bands which can yield large σ along with promising thermopower (S) enabling optimum power-factor values ($S^2\sigma$). Figure 7 shows the variation of σ , $S^2\sigma$, κ_e and ZT as a function of carrier concentration at different temperatures for both p-type and n-type conduction of semi-metallic $\text{Cu}_2\text{ZnGeTe}_4$. In the present case, we have used

constant relaxation time approximation ($\tau = 80$ fs for holes and $\tau = 60$ fs for electrons) to simulate the thermoelectric properties due to the semi-metallic nature of the band structure, where n- and p-type conduction are mixed-up.

As evident from figure 7, semi-metallic phase has higher values of power-factor and electronic thermal conductivity due to their high mobility. At room temperature, and at a fixed carrier concentration of $1 \times 10^{20} \text{ cm}^{-3}$, the values of S , σ and $S^2\sigma$ are $85.5 \mu\text{V/K}$, $5.6 \times 10^5 \Omega^{-1}\text{m}^{-1}$ and $4.1 \text{ mWm}^{-1}\text{K}^{-2}$ respectively leading to a ZT value of 0.2. When compared with other semi-metals reported so far, this turn out to be a reasonably large ZT value at room temperature. At higher temperatures, the ZT value further increases to ~ 0.36 for p-type conduction at a carrier concentration of $6 \times 10^{20} \text{ cm}^{-3}$ as shown in Fig. 7(d). For n-type conduction, the maximum ZT (~ 0.24) arises at 800 K at a carrier concentration of $4 \times 10^{20} \text{ cm}^{-3}$. In the next section, we will show how alloy engineering can help to achieve the desired volumetric

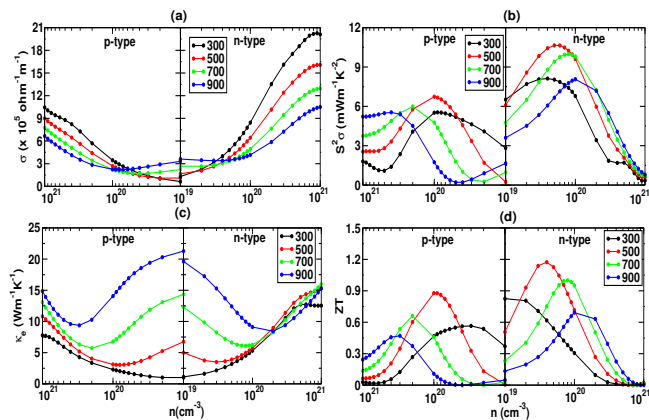


FIG. 6. For $\text{Cu}_2\text{ZnGeTe}_4$ (in semi-conducting state), carrier concentration (n) dependence of (a) electrical conductivity (σ), (b) power factor ($S^2\sigma$), (c) electronic thermal conductivity (κ_e) and (d) TE figure of merit (ZT) at different temperature (T) for p-type (left) and n-type (right) conduction.

change and hence the topological semi-metal phase without the application of externally applied pressure.

IV. ALLOY ENGINEERING

We explored the effect of selective substitution/doping in $\text{Cu}_2\text{ZnGeTe}_4$ to drive the system to topological non-trivial state. The substitutional site was chosen carefully so as not to affect the band topology much at/near the E_F . Ge is an ideal site whose contribution at/near the E_F is small, see the density of states plots figures 3(b,d). We found that with 50% substitution of Sn at Ge site, the system shows topological non-trivial feature as shown in Figure 8. The theoretically optimized volume of 50% Sn substituted $\text{Cu}_2\text{ZnGeTe}_4$ is 461.9 \AA^3 . The band-topology is not affected much apart from the fact, that the conduction band minima at X point which was four-

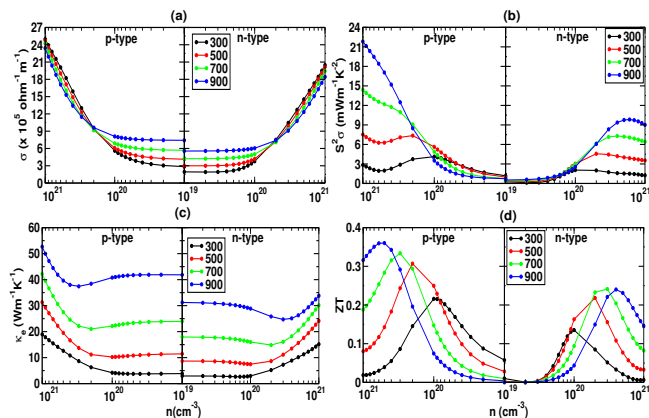


FIG. 7. For $\text{Cu}_2\text{ZnGeTe}_4$ (in semi-metallic state), carrier concentration (n) dependence of (a) σ (b) $S^2\sigma$, (c) κ_e and (d) ZT at different T for p-type (left) and n-type (right) conduction.

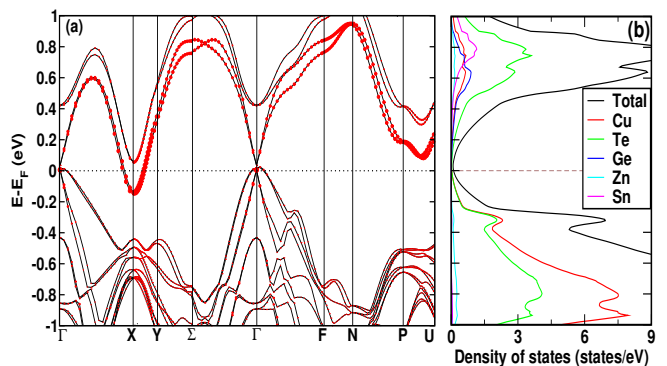


FIG. 8. Electronic band structure and total/atom-projected density of states of $\text{Cu}_2\text{ZnGe}_{0.5}\text{Sn}_{0.5}\text{Te}_4$.

fold degenerate in Fig. 3(a,c) now split into two doubly-degenerate bands. The topological non-trivial features including band inversion, Weyl nodes, chirality and robust surface states in the present case resemble that of the strained case shown earlier. Thus, apart from strain, alloy engineering can also help in achieving topological non-trivial semi-metallic state while retaining the nature of band topology and band convergence criteria almost intact required for promising TE properties.

V. CONCLUSION

In summary, we have predicted the simultaneous existence of topological Weyl semi-metal and promising thermoelectric properties in $\text{Cu}_2\text{ZnGeTe}_4$. This system is a narrow band gap (0.067 eV) semiconductor at ambient condition which transforms to topological Weyl semi-metal under external pressure as well as alloying with Sn. Both the phases have low lattice thermal conductivity, beneficial for TE performance. The semiconducting phase show a reasonably high TE figure of merit (ZT) ~ 1.2 for n-type conduction. The topological non-trivial semi-metal feature (under external pressure) is confirmed by band inversion, opposite chirality and robust surface states. This semi-metal phase also show decent ZT value of 0.36 (p-type) due to presence of both linear and regular parabolic bands at/near the Fermi-level (E_F). 50% Sn substitution in $\text{Cu}_2\text{ZnGeTe}_4$ also drives the system to topological Weyl semi-metal phase. We strongly believe that the present study will motivate the community to further explore the novel topological semi-metallic systems for thermoelectric applications, which has been rare.

VI. ACKNOWLEDGEMENTS

B.S. acknowledges computing facilities (spacetime) of IIT Bombay to carry out the calculations. A.A. acknowledges DST-SERB (Grant No. CRG/2019/02050)

for funding to support this research.

* aftab@iitb.ac.in

- ¹ T. M. Tritt, Thermoelectrics Run Hot and Cold, *Science* **272**, 1276 (1996).
- ² F. J. DiSalvo, Thermoelectric Cooling and Power Generation, *Science* **285**, 703 (1999).
- ³ D. Y. Chung, T. H. Hogan, P. Brazis, M. Rocci-Lane, C. Kannewurf, M. Bastea, C. Uher, M. G. Kanatzidis, CsBi₄Te₆: A High-Performance Thermoelectric Material for Low-Temperature Applications, *Science* **287**, 1024 (2000).
- ⁴ R. T. Littleton IV, T. M. Tritt, J. W. Kolis, D. R. Ketchum, Transition-metal pentatellurides as potential low-temperature thermoelectric refrigeration materials, *Phys. Rev. B* **60**, 13453 (1999).
- ⁵ G. S. Nolas, M. Kaeser, R. T. Littleton IV, T. M. Tritt, High figure of merit in partially filled ytterbium skutterudite materials, *Appl. Phys. Lett.* **77**, 1855 (2000).
- ⁶ B. C. Sales, D. Mandrus, R. K. Williams, Filled Skutterudite Antimonides: A New Class of Thermoelectric Materials, *Science* **272**, 1325 (1996).
- ⁷ J. J. G. Moreno, J. Cao, M. Fronzi, M. H. N. Assadi, A review of recent progress in thermoelectric materials through computational methods, *Materials for Renewable and Sustainable Energy* **9**, 16 (2020).
- ⁸ L. Huang, Q. Zhang, B. Yuan, X. Lai, X. Yan, Z. Ren, Recent progress in half-Heusler thermoelectric materials, *Materials Research Bulletin* **76**, 107 (2016).
- ⁹ A. L. Pope, T. M. Tritt, M. A. Chernikov, M. Feuerbacher, Thermal and electrical transport properties of the single-phase quasicrystalline material: Al_{70.8}Pd_{20.9}Mn_{8.3}, *Appl. Phys. Lett.*, **75**, 1854 (1999).
- ¹⁰ Chenguang Fu , Haijun Wu , Yintu Liu , Jiaqing He , Xinbing Zhao , Tiejun Zhu, Enhancing the Figure of Merit of Heavy-Band Thermoelectric Materials Through Hierarchical Phonon Scattering, *Adv. Sci.*, **3**, 1600035 (2016).
- ¹¹ Li You, Yefeng Liu, Xin Li, Pengfei Nan, Binghui Ge, Ying Jiang, Pengfei Luo, Shanshan Pan, Yanzhong Pei, Wenqing Zhang, G. Jeffrey Snyder, Jiong Yang, Jiye Zhang, Jun Luo, Boosting the thermoelectric performance of PbSe through dynamic doping and hierarchical phonon scattering, *Energy Environ. Sci.*, **11**, 1848 (2018).
- ¹² Min Hong, Yuan Wang, Tianli Feng, Qiang Sun, Shengduo Xu, Syo Matsumura, Sokrates T. Pantelides, Jin Zou, Zhigang Chen Strong Phonon-Phonon Interactions Securing Extraordinary Thermoelectric Ge_{1-x}Sb_xTe with Zn-Alloying-Induced Band Alignment, *J. Am. Chem. Soc.*, **141**, 4, 1742 (2019).
- ¹³ C. Kittel, "Introduction to Solid State Physics. 8th edn, John Willey and Sons." (2004).
- ¹⁴ Y. Pei, X. Shi, A. LaLonde, H. Wang, L. Chen, G. J. Snyder, Convergence of electronic bands for high performance bulk thermoelectrics, *Nature* **473**, 66 (2011).
- ¹⁵ Z. M. Gibbs, F. Ricci, G. Li, H. Zhu, K. Persson, G. Ceder, G. Hautier, A. Jain, G. J. Snyder, Effective mass and Fermi surface complexity factor from ab initio band structure calculations, *npj Comput. Mater* **3**, 8 (2017).
- ¹⁶ H. Zhang, C.-X. Liu, X.-L. Qi, X. Dai, Z. Fang and S.-C. Zhang, Topological insulators in Bi₂Se₃, Bi₂Te₃ and Sb₂Te₃ with a single Dirac cone on the surface, *Nat. Phys.* **5**, 438 (2009).
- ¹⁷ D. Hsieh, Y. Xia, D. Qian, L. Wray, F. Meier, J. H. Dil, J. Osterwalder, L. Patthey, A. V. Fedorov, H. Lin, *et al.*, Observation of Time-Reversal-Protected Single-Dirac-Cone Topological-Insulator States in Bi₂Te₃ and Sb₂Te₃, *Phys. Rev. Lett.* **103**, 146401 (2009).
- ¹⁸ T. H. Hsieh, H. Lin, J. Liu, W. Duan, A. Bansil and L. Fu, Topological crystalline insulators in the SnTe material class, *Nat. Commun.* **3**, 982 (2012).
- ¹⁹ Y. L. Chen, J. G. Analytis, J.-H. Chu, Z. K. Liu, S.-K. Mo, X. L. Qi, H. J. Zhang, D. H. Lu, X. Dai, Z. Fang, S. C. Zhang, I. R. Fisher, Z. Hussain, and Z.-X. Shen, Experimental Realization of a Three-Dimensional Topological Insulator, Bi₂Te₃, *Science* **325**, 178–181 (2009).
- ²⁰ J. Zhang, C.-Z. Chang, Z. Zhang, J. Wen, X. Feng, K. Li, M. Liu, K. He, L. Wang, Xi Chen, *et al.*, Band structure engineering in (Bi_{1-x}Sb_x)₂Te₃ ternary topological insulators, *Nat. Commun.* **2**, 574 (2011).
- ²¹ Ian T. Witting, Thomas C. Chasapis, Francesco Ricci, Matthew Peters, Nicholas A. Heinz, Geoffroy Hautier, and G. Jeffrey Snyder, The Thermoelectric Properties of Bismuth Telluride, *Adv. Electron. Mater.*, **5**, 1800904 (2019).
- ²² N. P. Armitage, E. J. Mele, and A. Vishwanath, Weyl and Dirac semimetals in three-dimensional solids, *Rev. Mod. Phys.* **90**, 015001 (2018).
- ²³ M. Markov, X. Hu, H.-C. Liu, N. Liu, J. Poon, K. Esfarjani, and M. Zebarjadi, Semi-metals as potential thermoelectric materials, *Sci. Rep.* **8**, 9876 (2018).
- ²⁴ Y. Pan, F.-R. Fan, X. Hong, B. He, C. Le, W. Schnelle, Y. He, K. Imasato, H. Borrmann, C. Hess, *et al.*, Thermoelectric Properties of Novel Semimetals: A Case Study of YbMnSb₂, *Adv. Mater.* **33**, 2003168 (2021).
- ²⁵ M. Theelen, F. Daume, Stability of Cu(In,Ga)Se₂ solar cells: A literature review, *Solar energy*, **133**, 586 (2016).
- ²⁶ X. Liu, T. Najam, G. Yasin, M. Kumar, M. Wang, One-Pot Synthesis of High-Performance Tin Chalcogenides/C Anodes for Li-Ion Batteries, *ACS Omega* **6**, 27, 17391–17399 (2021).
- ²⁷ M. Hong, Z.-G. Chen and J. Zou, Fundamental and progress of Bi₂Te₃-based thermoelectric materials, *Chinese Phys. B* **27** 048403, (2018).
- ²⁸ P. Kush, S. Deka, Multifunctional Cu-based Quaternary Chalcogenide Semiconductors Toward State-of-the-Art Energy Applications, *ChemNanoMat*, **5**, 373 – 402 (2019).
- ²⁹ B. Mukherjee, E. Isotta , C. Fanciulli, N. Ataollahi and P. Scardi, Topological Anderson Insulator in Cation-Disordered Cu₂ZnSnS₄, *Nanomaterials* **11**, 2595 (2021).
- ³⁰ M.- L. Liu, F.- Q. Huang, L.- D. Chen, and I- W. Chen, A wide-band-gap p-type thermoelectric material based on quaternary chalcogenides of Cu₂ZnSnQ₄ (Q=S, Se), *Applied Physics Lett.* **94**, 202103, (2009).
- ³¹ X. Y. Shi, F. Q. Huang, M. L. Liu, and L. D. Chen, Thermoelectric properties of tetrahedrally bonded wide-gap stannite compounds Cu₂ZnSn_{1-x}In_xSe₄. *Applied Physics Lett.* **94**, 122103, (2009).

- ³² Min-Ling Liu, I-Wei Chen, Fu-Qiang Huang, and Li-Dong Chen. Improved thermoelectric properties of Cu-doped quaternary chalcogenides of $\text{Cu}_2\text{CdSnSe}_4$. *Advanced Materials*, 3808–3812, (2009).
- ³³ P. Hohenberg and W. Kohn, Inhomogeneous Electron Gas, *Phys. Rev.* **136**, B865 (1964).
- ³⁴ G. Kresse and J. Furthmüller, Efficiency of Ab-Initio Total Energy Calculations for Metals and Semiconductors Using a Plane-Wave Basis Set. *Computational Materials Science, Comput. Mater. Sci.* **6**, 15 (1996).
- ³⁵ G. Kresse and J. Furthmüller, Efficient iterative schemes for ab initio total-energy calculations using a plane-wave basis set, *Phys. Rev. B* **54**, 011169 (1996).
- ³⁶ G. Kresse and J. Hafner, Ab initio molecular dynamics for liquid metals, *Phys. Rev. B* **47**, 558 (1993).
- ³⁷ J. P. Perdew, K. Burke, M. Ernzerhof, Generalized Gradient Approximation Made Simple, *Phys. Rev. Lett.* **78**, 1396 (1997).
- ³⁸ M. Ernzerhof and G. E. Scuseria, Assessment of the Perdew–Burke–Ernzerhof exchange–correlation functional, *J. Chem. Phys.* **110**, 5029 (1999).
- ³⁹ J. P. Perdew, M. Ernzerhof, K. Burke, Rationale for mixing exact exchange with density functional approximations, *J. Chem. Phys.* **105**, 9982 (1996).
- ⁴⁰ A. Becke, Density-functional thermochemistry. III. The role of exact exchange, *The Journal of Chemical Physics*, **98**, 5648 (1993).
- ⁴¹ J. Heyd and G. E. Scuseria, Hybrid functionals based on a screened Coulomb potential, *J. Chem. Phys.* **118**, 8207 (2003).
- ⁴² P. E. Blöchl, Projector augmented-wave method, *Phys. Rev. B* **50**, 17953 (1994).
- ⁴³ A. V. Krukau, O. A. Vydrov, A. F. Izmaylov, and G. E. Scuseria, Influence of the exchange screening parameter on the performance of screened hybrid functionals, *The Journal of Chemical Physics* **125**, 224106 (2006).
- ⁴⁴ A. M. Ganose, J. Park, A. Faghaninia, R. Woods-Robinson, K. A. Persson, A. Jain, Efficient calculation of carrier scattering rates from first principles, *Nat. Commun.* **12**, 2222 (2021).
- ⁴⁵ O.V. Parasyuk, I.D. Olekseyuk, L.V. Piskach, X-ray powder diffraction refinement of $\text{Cu}_2\text{ZnGeTe}_4$ structure and phase diagram of the Cu_2GeTe_3 – ZnTe system *Journal of Alloys and Compounds* **397**, 169 (2005)
- ⁴⁶ H. B. Nielsen and M. Ninomiya, A no-go theorem for regularizing chiral fermions, *Phys. Lett. B* **105**, 219 (1981).
- ⁴⁷ M. T Dove and H. Fang, Negative thermal expansion and associated anomalous physical properties: review of the lattice dynamics theoretical foundation , *Rep. Prog. Phys.* **79**, 066503 (2016).
- ⁴⁸ See Supplemental Material at [URL will be inserted by publisher] which provide auxiliary information about the relaxation time formalism.
- ⁴⁹ J. J. Gong, A. J. Hong, J. Shuai, L. Li, Z. B. Yan, Z. F. Ren, J.- M. Liu, Investigation of the bipolar effect in the thermoelectric material CaMg_2Bi_2 using a first-principles study, *Phys. Chem. Chem. Phys.* **18**, 16566 (2016).